12th International Conference on Applications of Statistics and Probability in Civil Engineering, ICASP12
Vancouver, Canada, July 12-15, 2015

Shaking Table Experiment of Fault-Tolerant Seismic Vibration Control of a Building Based on Sensor Reliability

S. Tanaka
Graduate Student, Graduate School of Science and Technology, Keio University, Yokohama, Japan
M. Kohiyama
Associate Professor, Graduate School of Science and Technology, Keio University, Yokohama, Japan

ABSTRACT: The authors propose a compensation method using the Kalman filter and sensor reliability parameters to assure the continuous performance of vibration control even if sensor failures occur. The effectiveness of the proposed method was verified by conducting a shaking table test using a three-story specimen with an active mass damper, which is a small-scale model of a 15-story building. As a result of the shaking table test with simulated sensor damage, it was confirmed that the responses of inter-story drift angle and absolute acceleration were reduced by the proposed compensation method in comparison with a case without the proposed method.

Recently, seismic vibration control systems have been installed in many buildings to mitigate structural damage caused by severe ground motion. However, the control performance is only assured under the condition that all components, such as installed sensors and cables, work properly. If the sensors or cables are damaged for some reason, it is more difficult to suppress building vibrations and secure the people and property in the building.

Huang et al. (2007, 2012) proposed a redundant system against faults in linear drive systems. However, the proposed system requires that the sensors do not fail and the state of failure is described using a linear differential equation. Moseler and Isermann (2000) also proposed a way to detect faults in direct-current servo motor systems using the parameter evaluated by the Kalman filter. However, they did not mention the compensation of failures in the system.

We proposed a compensation method using a sensor reliability parameter to avoid performance deterioration of seismic vibration control due to sensor failures (Tanaka and Kohiyama 2014). The reliability parameter is defined on the basis of the difference between data acquired by sensors and data estimated by an observer.

To verify the proposed method with not only numerical simulations but also experiments, we designed a three-story specimen, and conducted shaking table experiments to clarify the effectiveness of the proposed method. This paper reports the results of those experiments, in which it was assumed that one of the installed sensors had a failure and data could not be acquired continuously.

1. FAULT-TOLERANT CONTROL

1.1. Reliability parameter

We introduced a reliability parameter r on the basis of Tanaka and Kohiyama (2014) defined as follows:

$$r(k) = \frac{1}{1+\dfrac{\sigma_e^2(k)}{\sigma_s^2(k)}} = \frac{\sigma_y^2(k)+\sigma_n^2(k)}{\sigma_y^2(k)+\sigma_f^2(k)+2\sigma_n^2(k)} \quad (1)$$

where $\sigma_X^2(k)$ represents the variance of the random process X (X can be s, e, y_h, y, n, or f) at discrete time k. We defined $s(k)$ as the true value, $e(k)$ as the deviation between the true and estimated values, $y_h(k)$ as the estimated value,

$y(k)$ as the observed value, $n(k)$ as the noise, and $f(k)$ as the deviation between the observed and estimated values. Using the reliability parameter defined in Eq. 1, the reliability parameter vector is defined as follows:

$$\mathbf{r}(k) = [r_1(k) \quad r_2(k) \quad \cdots \quad r_{N_s}(k)]^{\mathrm{T}} \tag{2}$$

where N_s is the total number of sensors installed in a building.

1.2. Algorithm for data compensation

1.2.1. State equation

We considered a model of a three-story building with an active mass damper (AMD) on the top floor as shown in Figure 1. The discretized state equation at discrete time k is as follows:

$$\begin{cases} \mathbf{x}_e(k+1) = \mathbf{A}_e\mathbf{x}_e(k) + \mathbf{B}_e u(k) + \mathbf{D}_e w(k) \\ \mathbf{y}_e(k) = \mathbf{C}_e\mathbf{x}_e(k) + \mathbf{E}_e u(k) + \mathbf{v}(k) \end{cases}, \tag{3}$$

where

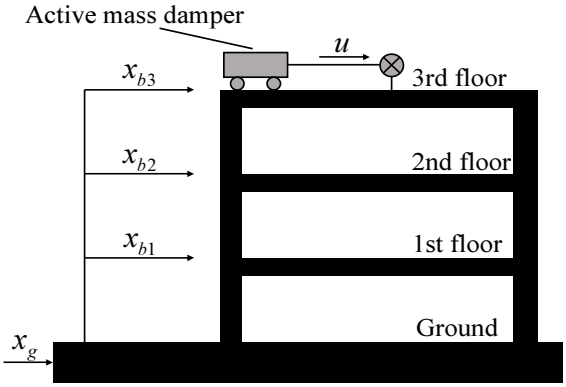

Figure 1: Three-story building model with AMD on the top floor

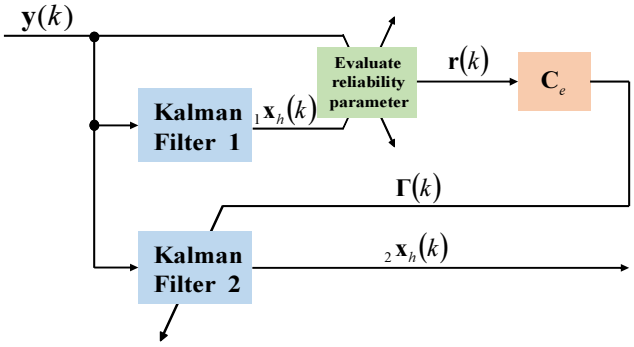

Figure 2: Block diagram to compensate for the lack of data due to sensor failures

$$\mathbf{x}_e = [x_{b1}\ x_{b2}\ x_{b3}\ \dot{x}_{b1}\ \dot{x}_{b2}\ \dot{x}_{b3}\ \dot{x}_g\ \ddot{x}_g]^{\mathrm{T}}, \tag{4}$$

$$\mathbf{A}_e = \left[\begin{array}{c|c} \mathbf{A}_o & \mathbf{D}_o\mathbf{C}_z \\ \hline \mathbf{O}_{(2\times 6)} & \mathbf{A}_z \end{array}\right], \quad \mathbf{B}_e = \begin{bmatrix} \mathbf{B}_o \\ \mathbf{O}_{(2\times 1)} \end{bmatrix}, \tag{5),(6}$$

$$\mathbf{C}_e = \begin{bmatrix} [0\ 0\ 0\ 1\ 0\ 0\ 1\ 0]\mathbf{A}_e \\ [0\ 0\ 0\ 0\ 1\ 0\ 1\ 0]\mathbf{A}_e \\ [0\ 0\ 0\ 0\ 0\ 1\ 1\ 0]\mathbf{A}_e \\ [0\ 0\ 0\ 0\ 0\ 0\ 0\ 1] \end{bmatrix}, \tag{7}$$

$$\mathbf{D}_e = \begin{bmatrix} \mathbf{O}_{(6\times 1)} \\ \mathbf{d} \end{bmatrix}, \quad \mathbf{E}_e = \begin{bmatrix} \mathbf{E}_o \\ 0 \end{bmatrix}, \text{ and} \tag{8), (9}$$

$$\mathbf{y}_e = [\ddot{x}_1 + \ddot{x}_g \quad \ddot{x}_2 + \ddot{x}_g \quad \ddot{x}_3 + \ddot{x}_g \quad \ddot{x}_g]^{\mathrm{T}}. \tag{10}$$

The definition of these matrices and variables follow those in Tanaka and Kohiyama (2014).

1.2.2. The proposed method for data compensation

The block diagram of the proposed method is described in Figure 2. Calculating the reliability parameter vector $\mathbf{r}(k)$, the time-variant observation matrix $\mathbf{\Gamma}(k)$ is updated by multiplying $\mathbf{r}(k)$, which consists of a reliability weighting factor at each discrete time k. This operation is described as follows:

$$\mathbf{\Gamma}(k) = \mathbf{r}(k)\mathbf{C}_e. \tag{11}$$

Vectors ${}_1\mathbf{x}_h$ and ${}_2\mathbf{x}_h$ are the estimated state vector using sensor-acquired values and the re-calculated state vector based on the proposed method, respectively.

2. EXPERIMENTAL VERIFICATION

2.1. Specimen

As a target building, we considered a 15-story building with a vibration control system. The physical parameters of the building are described in Table 1. Table 2 explains scaled parameters for the specimen. We designed a three-story model, in which we considered response vibration up to the third mode. A photograph and dimensions of the specimen are shown in Figure 3 and Table 3, respectively.

Table 1: Physical parameters of models

Parameter	Symbol	Full-scale model	Experimental model
Story height	h	4.0 m	0.306 m
Number of stories	N_f	15	3
Fundamental period	T_1	2 s	0.400 s*
First mode damping factor	ζ_1	0.02	0.0101*
Mass of each layer	m_{bi}	1.00×10^6 kg	m_{b1}: 4.47 kg m_{b2}: 4.37 kg m_{b3}: 4.57 kg
Maximum torque of controller	$u_{\max}$	21.5 kN·m	0.48 N·m

*The values were estimated by system identification.

Table 2: Scaled parameters for the specimen

	Full-scale model	Experiment model
Damping factor	ξ	ξ
Natural frequency	f	$5f$
Displacement	x	$x/5$
Acceleration	a	$5a$
Phase	θ	θ
Time	t	$t/5$
Mass	M_a	M_s
Force	$M_a \cdot a$	$M_s \cdot 5a$

Figure 3: Experimental Specimen

Table 3: Dimensions of the specimen

Parameter	Value
Specimen height	0.918 m
Specimen weight	13.41 kg

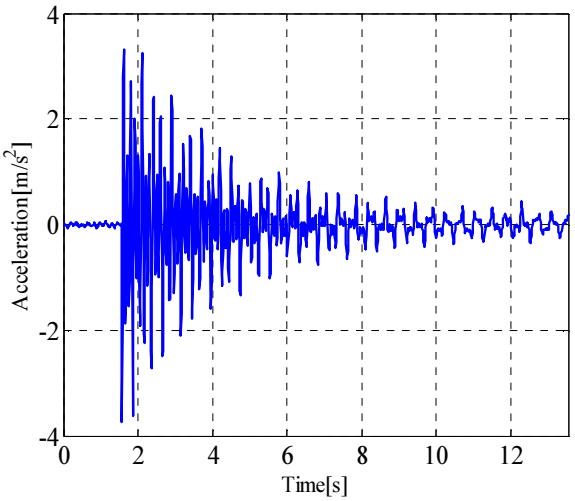

Figure 4: Time history of impulse response

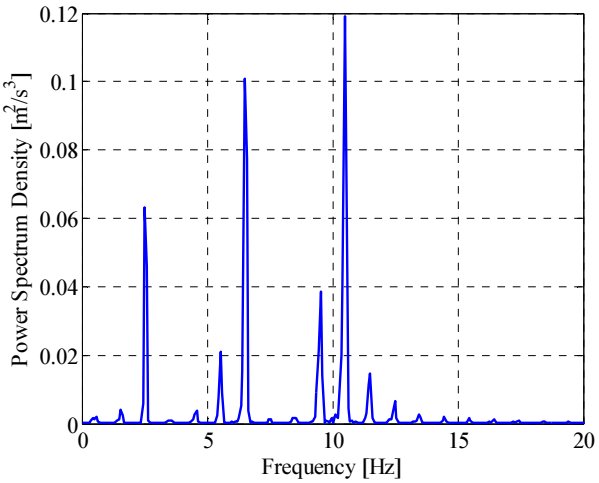

Figure 5: One-side power spectrum of impulse response

The specimen was scaled down on the basis of Watanabe et al. (2012). Time and displacement of the specimen are scaled by 1/5, and the mass and stiffness of the specimen are adjusted to match the scaled natural frequencies as shown in Table 2. The physical parameters of the specimen are shown in Table 1.

2.2. System identification

To accurately estimate the vibration characteristics of the designed specimen, we conducted a system identification experiment. First, an impulse force was applied to the top floor and we observed the time history of the acceleration response at the sensor installed on the top floor (Figure 4) and we calculated the first-mode damping factor. Then, the one-side power spectrum was evaluated using data acquired on the time history of the impulse response as shown in Figure 5. Based on the power spectrum, we estimated the natural frequencies and other model parameters of the specimen as shown in Table 4. Note that the sampling frequency is 100 Hz and the Nyquist frequency is 50 Hz. Damping factors were not directly identified and a proportional stiffness damping model was used with the identified first-mode damping factor using the following equation:

$$\mathbf{C}_b = \frac{2\zeta_1}{\omega_1}\mathbf{K}_b . \tag{12}$$

Table 4: Identified model parameters

Parameter	Symbol	Identified value
Natural period of specimen	T_1	0.400 s
	T_2	0.156 s
	T_3	0.0952 s
Stiffness coefficient	k_{b1}	4.90×10^3 N/m
	k_{b2}	4.90×10^3 N/m
	k_{b3}	3.79×10^3 N/m
Damping coefficient	c_{b1}	4.87 Ns/m
	c_{b2}	7.64 Ns/m
	c_{b3}	6.30 Ns/m

Table 5: Instruments of control system

Component	Instrument used
Linear slider	THK VLAST45
AC servo motor	Mitsubishi Electric HF-KP053
Acceleration sensor	Showa Sokki Model-2431
Digital signal processer	dSPACE DS1104-CP1104
Software for control	MathWorks MATLAB 2012a Real-Time Workshop
Computer for control	Dell Dimension 9150

2.3. Instruments

The instruments used in the experiments are listed in Table 5. Table 6 shows the specification of an alternating current (AC) servo motor for an AMD, which applies control force to the top floor as a reaction force by moving a mass on a linear slider. The allocation of acceleration sensors and an AMD is shown in Figure 6.

2.4. Input excitation

As input excitation, we used design ground motion prescribed by Notification No. 1461 of the Ministry of Construction, Japan, May 31, 2000, which is used in analyzing the time history response of high-rise buildings and base-isolated buildings in Japan, as shown in Figure 7. The absolute acceleration spectra of the input excitation are shown in Figure 8. A red curve in

Table 6: Specification of AC servo motor

Parameter	Value
Rated speed	3000 rpm
Maximum speed	6000 rpm
Torque at rated speed	0.16 N·m
Torque at maximum speed	0.48 N·m
Mass	0.35 kg
Moment of inertia	5.2×10^{-6} kg·m^2

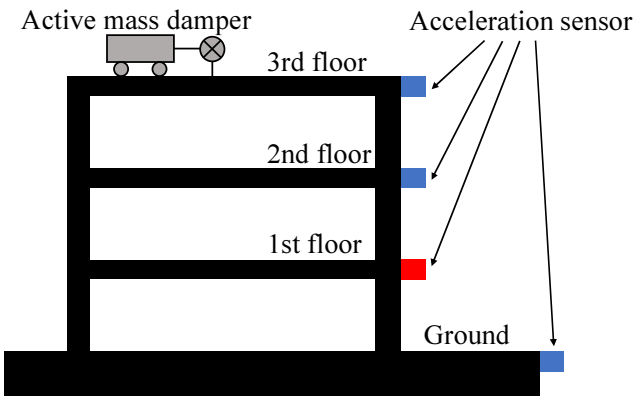

Figure 6: Sensors' allocation

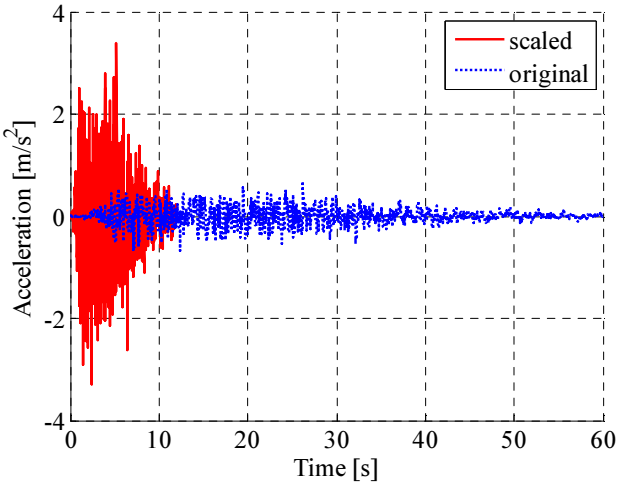

Figure 7: Comparison of acceleration time history between the original and scaled input excitation.

both figures shows the scaled excitation for the specimen. The maximum acceleration of the scaled excitation is 5 times larger than that of the original one, and the duration of the scaled input is a fifth of the original one.

2.5. Control system design

We introduced a linear quadratic Gaussian controller to suppress the response of the specimen. The control objective is to minimize the inter-story drift angle of the specimen. Then, we defined a cost function to obtain a gain for the optimal control force, which is applied to the top floor with an AMD, on the basis of the control objective.

The cost function is formulated as follows:

$$J = \sum_{k=1}^{\infty} \left(\mathbf{x}^{\mathrm{T}}(k)\mathbf{Q}\,\mathbf{x}(k) + R u^2(k) \right), \tag{13}$$

where

$$\mathbf{Q} = \mathbf{T}^{\mathrm{T}}\mathbf{T}, \tag{14}$$

$$\mathbf{T} = \frac{1}{h}\begin{bmatrix} 1 & 0 & 0 & 0 & 0 & 0 & 0 & 0 \\ -1 & 1 & 0 & 0 & 0 & 0 & 0 & 0 \\ 0 & -1 & 1 & 0 & 0 & 0 & 0 & 0 \end{bmatrix}, \tag{15}$$

and $R = 10^{-4}$. Using the optimal feedback gain $\mathbf{K}$, the optimal control force is given as:

$$u = -\mathbf{K}\mathbf{x}\,. \tag{16}$$

Note that the feedback gain $\mathbf{K}$ is derived by solving the Riccati equation, and the observability of the pair ($\mathbf{Q}$, $\mathbf{A}_e$) is assured.

2.6. Experiment

To verify the effectiveness of the proposed compensation method under the circumstance of sensor failures, we conducted three types of experiments as follows:

- Uncontrolled (Case 1)
- Controlled without compensation by the proposed method (Case 2)
- Controlled with compensation by the proposed method (Case 3)

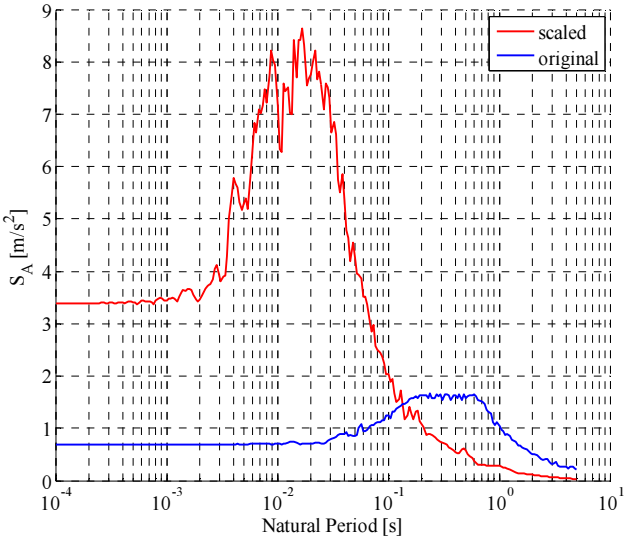

Figure 8: Comparison of absolute acceleration response spectra between the original and scaled input excitation.

We assume that an acceleration sensor installed on the first floor has a critical failure due to internal physical damage or cable disconnection in all cases. As a result, no information about the first floor acceleration is sent to the observer and controller. Therefore, the observer continuously acquires zero as the input for the first floor absolute acceleration. In Figure 6, the red sensor mark indicates a failed sensor, and the blue ones indicate intact sensors.

We conducted the same shaking table experiments 10 times to consider the error of input excitation reproducibility. Then, we compared the maximum and root mean square (RMS) values of the responses (inter-story drift angle and absolute acceleration) of each layer (or floor) among the three cases (Cases 1, 2, and 3).

The results of the experiments are shown in Table 7. We confirmed that the proposed method can compensate for the lack of data and avoid deterioration of control performance except for the absolute acceleration of the third floor. Case 1 (no control force) had the largest response among the three cases.

With respect to inter-story drift angle, in comparison with Cases 2 and 3, the improvement ratio of the maximum inter-story drift angle between the second and third floors is 32.5%.

Table 7: The results of the experiments

Maximum inter-story drift angle [rad]

	Ground–1st floor	1st floor–2nd floor	2nd floor–3rd floor
Case 1	0.828 (0.170)*	0.458 (0.130)	0.413 (0.107)
Case 2	0.719 (0.107)	0.406 (0.168)	0.360 (0.0945)
Case 3	0.589 (0.0934)	0.407 (0.103)	0.243 (0.0396)

RMS of inter-story drift angle [rad]

	Ground–1st floor	1st floor–2nd floor	2nd floor–3rd floor
Case 1	0.201 (0.0167)	0.108 (0.0156)	0.0872 (0.0135)
Case 2	0.176 (0.0137)	0.0961 (0.0200)	0.0754 (0.0149)
Case 3	0.152 (0.00663)	0.0924 (0.0145)	0.0616 (0.0104)

Maximum absolute acceleration [m/s^2]

	1st floor	2nd floor	3rd floor	Ground (input)
Case 1	9.27 (0.262)	6.59 (0.205)	5.37 (0.196)	2.81 (0.0948)
Case 2	8.24 (0.279)	6.88 (0.248)	5.69 (0.225)	2.83 (0.327)
Case 3	7.06 (0.464)	6.52 (0.305)	5.80 (0.254)	2.83 (0.150)

RMS of absolute acceleration [m/s^2]

	1st floor	2nd floor	3rd floor	Ground (input)
Case 1	2.27 (0.0555)	1.77 (0.0464)	1.43 (0.0317)	0.638 (0.00782)
Case 2	1.91 (0.0384)	1.59 (0.0257)	1.40 (0.0256)	0.648 (0.00900)
Case 3	1.62 (0.0425)	1.49 (0.0220)	1.41 (0.0410)	0.632 (0.0125)

Note: The value on the left shows an average and the value on the right in parentheses shows the standard deviation.

Similarly, the improvement ratio of RMS between the second and third floors is 18.3%.

With respect to absolute acceleration, in comparison with Cases 2 and 3, the improvement ratios of the maximum absolute accelerations of the first and second floors are 14.3% and 5.23%, respectively. Similarly, the improvement ratios of RMS at the first and second floors are 15.2% and 6.29%, respectively.

We did not confirm the reduction of absolute acceleration response at the third floor. This is because a moving mass of AMD, which moves according to the command signal of the control force, was occasionally hit on the rail end of a linear slider and thus, impact force was sometimes applied to the top floor. This impact force made it difficult to control the acceleration of the third floor.

3. CONCLUSIONS

To verify the effectiveness of the proposed compensation method based on sensor reliability parameters, we designed a three-story specimen of a small-scale model of a 15-story building with AMD and conducted shaking table experiments. As a result, we confirmed that the absolute acceleration of the first and second layers (stories) and the inter-story drift angle were reduced more by applying the proposed compensation even in the case with sensor failures compared with a case without the proposed compensation method.

In future studies, we will conduct an experiment assuming multiple sensors are damaged. Moreover, we will study a reliable compensation method and robust control method for a vibration control system using a wireless sensor network.

ACKNOWLEDGEMENTS

This research was financially supported by the Japan Society for Promotion of Science KAKENHI Grant-in-Aid for Scientific Research (B) 24360230.

REFERENCES

Huang, S.N., Tan, K.K., and Lee, T.H. (2007). "Automated Fault Detection and Diagnosis in Mechanical Systems" *IEEE Transactions on Systems, Man, and Cybernetics–Part C: Applications and Reviews*, 37(6), pp. 1360–1364.

Huang, S., Tan, K.K., and Lee, T.H. (2012). "Fault Diagnosis and Fault-Tolerant Control in Linear Drives Using the Kalman Filter" *IEEE Transactions on Industrial Electronics*, 59(11), pp. 4285–4292.

Moseler, O. and Isermann, R. (2000). "Application of Model-Based Fault Detection to a Brushless DC Motor" *IEEE Transactions on Industrial Electronics*, 47(5), pp. 1015-1020.

Tanaka, S. and Kohiyama, M. (2014). "Fault-tolerant seismic vibration control of a building with sensor reliability evaluated by the Kalman Filter" *Proc. 4th International Symposium on Life-Cycle Civil Engineering*, Tokyo, Japan, DVD, pp. 1140–1146.

Watanabe, K., Miura, N., Kohiyama, M., and Takahashi, M. (2012). "Experimental research of seismic response control of building-elevator system using linear quadratic Gaussian controller" *Proc. 9th International Conference on Urban Earthquake Engineering & 4th Asia Conference on Earthquake Engineering Joint Conference*, Tokyo, Japan, Paper No. 09-126, pp. 1527–1531, CD-ROM.